Peer-reviewed version available at Machines 2017, 5, 30; doi:10.3390/machines5040030

Article

Iron Loss Prediction Using Modified IEM-Formula during the Field Weakening for Permanent Magnet Synchronous Machines

Pedram Asef [1,*], Ramon Bargallo [1] and Andrew Lapthorn [2]

[1] The Department of Electrical Engineering, Polytechnic University of Catalonia-BarcelonaTech (UPC), Spain; ramon.bargallo@upc.edu
[2] The Department of Electrical and Computer Engineering, University Of Canterbury, Christchurch, New Zealand; andrew.lapthorn@canterbury.ac.nz
* Correspondence: pedram.asef@upc.edu; Tel.: +1-979-583-8666

Abstract: During field weakening operation time (FWOT), the total iron loss rises and affects the accuracy of loss prediction and efficiency especially if a large range of FWOT exists due to a large voltage drop which rooted from the resistance of the used material. Iron loss prediction is widely employed in investigations for a fast electrical machine analysis using 2-D FEA. This paper proposes harmonic loss analytically by a steady-state equivalent circuit with a novel procedure. Consideration of skin effects and iron saturation are utilized in order to examine the accuracy through the relative error distribution in the frequency domain of each model from 50 to 700 Hz. Additionally, this comparative study presents a torque-frequency-field density calculation over each single term of the modified IEM-formula. The proposed analytical calculation is performed using 2-D FEA for a classic and modified IEM-formula along with experimental verifications on a surface-mounted permanent magnet synchronous generator (PMSG) for a wind generation application.

Keywords: electrical machine; field weakening; IEM-formula; wind energy; iron loss; synchronous generator; equivalent circuit; harmonic loss

1. Introduction

Recently a modern distinguished iron loss formulation known as IEM-Formula by RWTH Aachen University in Germany has been proposed in order to deal with an advanced iron loss estimation on nonlinear materials such as soft magnetic materials for electrical machines [1-3]. The proposed IEM-Formula needed to be evaluated under field weakening condition because the field weakening capability plays a significant role in the iron loss prediction of permanent magnet synchronous machines (PMSMs) over a wide range of speed, particularly at high speeds.

There are a number of well-known articles for iron loss calculations with skin effect considerations [4-9]; however, only a few have considered field weakening capability.

Z. Haisen, et al., studied a two-term piecewise variable parameter model for precise prediction of iron losses in induction motors. They used also eddy-current terms of IEM-Formula, in which also skin effect has been accounted. The iron loss model has been numerically and experimentally verified, however, the model is not valid during FWOT, while harmonic loss is not considered [10].

In ref. [11], S. H. Han et al. reported the influence of harmonic losses to increase and dominate the total iron loss during field weakening operation. A useful comparative study on the produced harmonics and eddy-current loss (in the stator-teeth) is presented. Although, lack of experimental verification afflicted the quality of the research.

Q. Li et al., investigated the rotor saliency of an interior permanent magnet (IPM) machine, large harmonic eddy-current loss in the stator iron loss could be caused under field-weakening operation, conspicuously impairing the output performance of the IPM machine. They proposed a new stator teeth eddy-current loss analysis approach, in which the teeth eddy-current loss is divided

to two parts, one part is caused by the synchronous air-gap field density rotating synchronously with rotor, while the other part is induced by the asynchronous air-gap field density [12]. There is a though-provoking consideration on the fractional-slot concentrated winding based on the eddy-current coefficients, however, an experimental test needs to being considered. In addition the following works have been fully discussed the fractional-slot concentrated winding [13-14].

In [15] and [16], the iron loss resistance was calculated a priori from a finite-element analysis as functions of the d–q-axis currents. On the other hand, the effect of field-weakening current on the iron losses of the PMSM is presented in [17]. Further, FEA based iron loss calculation methods have been used to minimize the iron losses of the PMSM under field weakening condition in [18] and [19].

S. Kuttler et al. studied an original and mathematical model which has been developed and provides fast and accurate estimation of iron losses, particularly in field weakening operation, even with the machine supplied by sinusoidal currents as described in this work. A polynomial form of iron losses as function of fundamental electrical frequency and takes into account the filed density waveforms in the yoke and teeth by use of nonlinear iron coefficients linked to i_d–i_q currents. The paper has presented the complete method for calculating the iron coefficients from a nonlinear magnetic nodal network of the machine. A detailed study of the local field density waveform and harmonic content in the yoke and teeth was provided for two particular operating points: at maximal power without field weakening and at maximal power at maximal speed [20]. This article investigated mapping of local iron losses coefficients in yoke and teeth, and also the iron losses coefficients differences justified per unit volume between yoke and teeth. However, there was no experimental validation present in the article.

In ref. [21], a special design for a spoke-type IPM motor is presented to enhance motor field-weakening capability in operation over a wide speed range. Experimental results have been compared with analytical predictions showing satisfactory accordance. It can be concluded that calculation analysis with simulation and measurement results for motor operation through imposed voltage and torque profiles over the basic objectives is well presented.

In [22], the researchers dealt with the concept of winding switching for field weakening of PMSM. The study focused the impact of harmonic contents on the field weakening capability of the machine. Afterwards, a suitable drive topology for the winding switching technique under harmonic conditions is discussed. The technique as a field weakening solution was only investigated on the field and back-EMF. At last, the results are experimentally verified. Although, the iron loss consideration or influence of the proposed technique was not discussed, but the solution can be considerable for iron loss improvement during FWOT for further investigations. Moreover, ref. [23] proposed an improvement in the field weakening operation over a large speed range, in which power and torque have been raised.

In another research [24], the authors presented a special emphasis is placed on accurately representing core losses at variable frequency. The analytical model has been experimentally verified. Although, the lack of iron loss prediction namely during FWOT can be seen which can be considered to improve the accuracy during FWOT.

M. Basic et al. studied iron losses by means of an equivalent iron loss resistance which is connected in parallel with the stator inductance. Moreover, the iron loss resistance is modeled as variable with respect to both synchronous frequency and magnetizing field, whereas the magnetizing field influence is expressed by means of the corresponding iron loss current. Finally, a good achievement over the proposed model is carried out [25]. The research lacks field weakening capability, and also experimental verifications.

In this paper, the main focused is on harmonic loss consideration on the classic IEM-Formula, which significantly effects the iron loss prediction during FWOT. The objective can be reached through analytical improvement of harmonic loss modelling based on equivalent circuit for the IEM-Formula under flux weakening condition for the first time. In other words, a further analytical procedure and improvement over harmonic loss modelling for this formula is proposed as major contribution of this study. In order to improve the prediction of the iron losses in a surface mounted permanent magnet synchronous machine over a wide range of speed during FWOT, the harmonic

loss (rooted from steel sheets' resistance behavior), skin effect and field weakening capability are analytically and numerically defined into the formula, in which a number of coefficients are introduced, and thus calculated using conventional nonlinear curve fitting. Moreover, the influence of advanced iron loss prediction on the efficiency is taken into account. To avoid a time-consuming analysis, a 2-D-FEA is employed along with experimental result verifications to identify the modified IEM-Formula and verify its accuracy on a surface mounted permanent magnet synchronous generator. In the modified IEM-Formula model, the slot opening and fringing effects are neglected. The harmonic loss produced by the permanent magnets (PMs) and fundamental phase current are considered while; both phase current harmonic and inverter-carrier harmonic are ignored.

2. CLASSIC IEM-FORMULA EVALUATION

The classic IEM-Formula is introduced by D. Eggers [1-2] in 2012 in the following form:

$$P_{IEM}(B,f) = P_h + P_e + P_{exc} = a_1 B^{\alpha} f + a_2 B^2 f^2 (1 + a_3 B^{a4}) + a_5 B^{1.5} f^{1.5} \quad (1)$$

where a_1, a_2, a_3, a_4, and a_5 are the coefficients which will be estimated via nonlinear curve fitting. α is the fitted material parameter which is found using dc-measurements (quasi-static loss measurements using a field-meter) in a standard Epstein frame, finding the best parameter set describing the hysteresis losses as:

$$E_{DC} = a_1 . \hat{B}^{\alpha} \quad (2)$$

The classic formula is examined for M400-50A steel sheet between 50 to 700 Hz, and is compared to a standard Epstein frame test which is exhibited in Figure 1. The employed Epstein frame comprises a primary and a secondary winding. The sample is evaluated in a set of a number of strips cut from M400-50A steel sheet, in which each layer of the sample is double-lapped in corners and weighted down with a force of 1 N under the well-known International standard for the measurement configuration and conditions (IEC 60404-2:2008) magnetic materials. The iron loss prediction was predicted acceptable on the steel sheet parts of the machine (approximately linear) for a various range of frequencies (50-700 Hz), and up to 2 T.

Single-valued magnetization curves are employed to consider saturation effects (3) originating from the nonlinear material behavior. The magnetic material is utilized up to 2.1 T in the considered machine. Second-order effects, originating from hysteresis behavior, are neglected.

$$P_{sat.}(\hat{B},f) = a_2 . a_3 \hat{B}^{a_4+2} . f^2 \quad (3)$$

A. Skin Effect consideration

The eddy-current term of the classic formula is as:

$$P_e = a_2 B^2 f^2 (1 + a_3 B^{a_4}) \quad (4)$$

where the coefficient (a_2), which considers the skin effect by accounting for the thickness of the steel used, is:

$$a_2 = \frac{\pi^2 d^2}{6 \rho \rho_e} \quad (5)$$

with the sheet thickness (d), specific density (ρ) and specific electrical resistivity (ρ_e) of the soft magnetic material.

B. Steady-state Equivalent Circuit With Iron Loss Resistance Consideration

During FWOT, the importance of stator and rotor cores' resistance as well as its influence on the total iron loss is orderly defined into the d–q-axis equivalent circuit to examine the iron loss evaluation in advance. The steady-state equivalent circuit of the PMSM is shown in Figure 2 [24]. Moreover, the voltage drops $R_s I_d$ and $R_s I_q$ of the stator winding resistance are taken into account for the iron loss model based on the equivalent circuit, in which reference [27] assumed the winding resistance negligible. Although, its ohmic value can be large specially under field weakening condition. Therefore, a more accurate iron loss modelling rooted from both core and winding resistance consideration. The following expressions can be extracted from the equivalent circuit:

Preprints (www.preprints.org) | NOT PEER-REVIEWED | Posted: 24 October 2017 doi:10.20944/preprints201710.0155.v1

Peer-reviewed version available at Machines 2017, 5, 30; doi:10.3390/machines5040030

$$U_d = R_s I_d - \omega L_q I_{aq} \quad , \quad U_q = R_s I_q + \omega L_d I_{ad} + \omega \lambda_m$$
$$I_d = I_{ad} - I_{cd} \quad , \quad I_q = I_{aq} + I_{cq}$$
$$I_{cd} = \frac{\omega L_q I_{aq}}{R_c} \quad , \quad I_{cq} = \frac{\omega L_d I_{ad} + \omega \lambda_m}{R_c} \tag{6}$$
$$P_{fe} = \frac{3}{2}\frac{U_s^2 - (R_s I_d)^2}{R_c} \quad , \quad P_{fe} = \frac{3}{2}\frac{U_s^2 + (R_s I_q)^2}{R_c}$$
$$where \quad U_s = \sqrt{U_d^2 + U_q^2}$$

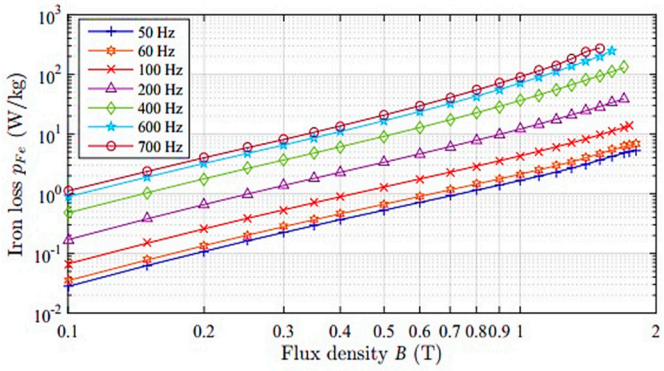

Figure 1. Comparison of five coefficients IEM-Formula with measurements under 50 up to 700 (Hz) frequencies from Epstein test

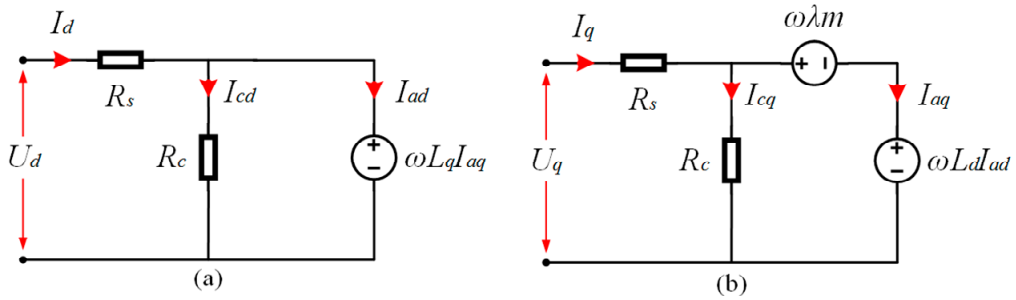

Figure 2. Steady-state equivalent d–q circuits of PMSM with iron loss resistance, listed as: (**a**) d-axis equivalent circuit; (**b**) q-axis equivalent circuit.

Referring to the above equations, the relation of the iron loss resistance to the magnetic field density waveforms (in the iron parts) can be derived from the analytical calculation of iron loss as follows:

$$P_{IEM} = [a_1 B_t^2 f + a_2 B_t^2 f^2 (1 + a_3 B_t^{a_4}) + a_5 B_t^{1.5} f^{1.5}] V_t$$
$$+[a_1 B_y^2 f + a_2 B_y^2 f^2 (1 + a_3 B_y^{a_4}) + a_5 B_y^{1.5} f^{1.5}] V_y \tag{7}$$

where V_t and V_y are the volume of the tooth and yoke in stator.

In a no-load condition, the iron loss P_{IEM1} is produced via the no-load fundamental air-gap field density component B_{m1} can be rewritten as follows:

$$P_{IEM1} = [a_1 B_{m1}^2 f k_{tf}(1)^2 + a_2 B_{m1}^2 f^2 k_{tf}(1)^2 (1 + a_3 B_{m1}^{a_4})] V_t$$
$$+[a_1 B_{m1}^2 f k_{yf}(1)^2 + a_2 B_{m1}^2 f^2 k_{yf}(1)^2 (1 + a_3 B_{m1}^{a_4})] V_y \tag{8}$$

Regarding to the analytical procedure, the magnetic induction is calculated once only for the stator yoke, and another time for stator teeth, hence k_{tf} as the teeth filter constant is defined:

$$k_{tf}(h) = \frac{\sin(h \alpha_s / 2)}{k_t . h . (\alpha_s / 2)} \tag{9}$$

where α_s is one tooth pitch angle, and k_t (the teeth-width coefficient) base on one tooth pitch (τ_s), and one tooth-pitch (b_t) can be calculated by:

$$k_t = \frac{b_t}{\tau_s} \tag{10}$$

Moreover, the magnetic induction calculation at the stator yoke requires another parameter which is yoke filter constant as:

$$k_{yf}(h) = \frac{\sin(\alpha_s/2)}{k_y.(\alpha_s/2)} \tag{11}$$

where k_y as the yoke-height coefficient is:

$$k_y = \frac{b_y}{\tau_p} \tag{12}$$

τ_p is the pole-pitch in the air-gap, and b_y is one yoke-pitch.

In no-load condition, assuming n current drawn from the machine supply which means $I_d = I_q = 0$, therefore the term $\omega\lambda_m$ forces an additional current $I_{aq} = -I_{cq}$ which is different from zero. Hence, due to the term $-\omega L_{aq} I_{aq}$ in the *d*-axis circuit, therefore a current as I_{ad}=-I_{cd} will be increased. What is more, the back-EMF term of $\omega L_{ad} I_{ad}$ is occurred in the *q*-axis. As a result, the total voltage across R_c (total stator core resistance) is not only equal to $\omega\lambda_m$, but also back-EMF terms of $-\omega L_{aq} I_{aq}$ and $\omega L_{ad} I_{ad}$ should be considered. Despite to this matter of fact, these voltage drops are ignored by the work done in reference [27], which causes a considerable error. The modified IEM-Formula which can be rewritten based on the steady-state equivalent circuit and equations (4) and (8) given as:

$$P_{IEM1} = 3/2\left((\omega\lambda_m - \omega L_{ad} I_{ad})^2 / R_c \right) \tag{13}$$

3. ANALYTICAL CONCEPT OF THE IRON LOSS MODEL WITH HARMONIC LOSS CONSIDERATIONS

During FWOT, the iron loss cannot be determined accurately using only the magnetic field density, because the terminal voltage is steady, being limited with DC link voltage. Regarding to this issue, a harmonic loss and voltage are induced at the tooth and yoke of the stator core which are analytically modelled (in Equation 6) based on the iron loss resistance. Therefore, a large eddy-current loss will be generated which critically decreases the efficiency, especially if a wide region of FWOT exists. Thus, the IEM-Formula model is adopted with a resistance model which considers harmonic loss. Harmonic loss is investigated through the air-gap magnetic field density harmonics from the elemental component and the machine's equivalent circuit parameters (shown in Figure 2), based on the air-gap field density analysis in [11] [26-27]. Therefore, the iron loss decreases in a similar manner during FWOT. Although, this predicted loss is far from the results from experiments and FEA computation. This is due to the fact that an important eddy-current loss will be generated at FWOT which significantly decreases the efficiency of the machine, this is also validated in [26] and [27]. The iron loss resistance model based on the IEM-Formula should be modified to consider harmonic loss during FWOT for the PMSM with closed-slot, double-layer fractional-slot concentrated winding [28-29].

Figure 3-a reveals the no-load air-gap magnetic field density (B_{mg}) and fundamental no load magnetic field density (B_{mg1}) by 3-D-FEA, and experimental verifications. Also, the no load air-gap magnetic field density harmonic waveform (B_{mg}) is shown in Figure 3-b. The waveform of B_{mg} for one pole range is shown in Figure 3-b along with its elemental component. The remaining harmonic component waveform of B_{mg} is demonstrated in Figure 3-b. For experimental measurement of the air-gap field density. It is required to wind search coils onto armature tooth tips of the tested generator to detect air-gap field. The d-axis pickup should be also installed at the generator to detect the number of revolutions and to synchronize the execution of a program with the revolutions. The d-axis pickup generates a pulse per electric cycle. In addition, the location of search coils at armature tooth tips and

at various parts of the rotor and the location of the d-axis and the d-axis pickup in the tested generator, the used methodology is validated in [30].

By a sinusoidal three-phase current excitation, the total air-gap field density [31] is written as:

$$B_g(\gamma,\omega t) = B_{mg0}(\gamma,\omega t) + B_{gr}(\gamma,\omega t) \quad (14)$$

where B_{mg0} and B_{gr} are the sum of the no-load magnetic field density and the armature reaction air-gap magnetic field density. For non-sinusoidal waveforms, the eddy-current term in (1) can be modified (based on [25-26]) to give the following expression:

$$P_e = a_{2'}\left[\frac{dB}{dt}\right]^{\alpha} + (1 + a_3 B^{a4}) \quad (15)$$

α is a coefficient which depends on the type and thickness of the laminated magnetic material. Also, $a_{2'} = a_2/(2\pi^2)$ is the new eddy-current coefficient, and [dB/dt] is the *rms*-value of the rate of change of field density over one cycle of the fundamental frequency [32].

Consequently, for the predicted iron loss produced in this condition, the influence of the harmonic component on the hysteresis loss is small (about 9% of total iron loss) under open-circuit condition. Hence, the modified eddy-current loss density in W/m² is proportional to the energy of the differential of the field density given as:

$$p_{eddy} = \frac{a_2}{2\pi^2 T}\int_0^T \left(\sum_{h\in 1,3,5,7}^{\infty} \frac{\partial B(\omega t)}{\partial t}\right)^{\alpha} dt + (1 + a_3 B^{a_4}) \quad (16)$$

The modified IEM-Formula based on the harmonic loss can be given by the machine's equivalent circuit parameters as:

$$P_{fe} = P_{IEM1} + P_{harmonic} = \frac{3}{2}\left(\frac{U_s^2}{R_c} + k_{ph}\frac{U_{ph}^2}{R_{ce}}\right) \quad (17)$$

where P_{IEM1} and P_h are the classic IEM-Formula and modified IEM-Formula (which considers iron loss resistance) and harmonic iron loss. k_{ph} is a harmonic coefficient to evaluate the harmonic field density range, which is adjusted via the machine design parameters, and U_{ph} is a harmonic voltage which refers to the ratio of the harmonic field density to the fundamental term.

$$P_h \propto \frac{4B_{sym}^2}{\pi}\sum_{h=3,5,\ldots}^{\infty} k_{sw}^2(1)k_{tf}^2(1)V_t + k_{sw}^2(1)k_{yf}^2(1)V_y \quad (18)$$

As the generated synchronous air-gap magnetic field density is caused from the fundamental air-gap field density (B_{g1}) and harmonic component B_{syh}, it can be expressed as:

$$B_{syh}(\gamma,\omega t) = \frac{4B_{sym}}{\pi}\sum_{h=3,5,\ldots}^{\infty}\frac{k_{sw}(h)}{h}\cos(h(\gamma - \omega t)) \quad (19)$$

$$B_{sym} = B_m - \frac{\mu_0}{g}k_U k_{pe}(1)\cos(\psi_1)F_{s1} \quad (20)$$

where F_{s1} is the fundamental magnetic motive force (MMF) in the stator, k_{sw} constant is a unit square function and through Fourier series can be developed to:

$$k_{sw}(h) = \sin\left(\frac{\alpha_p \pi h}{2}\right) \quad (21)$$

where α_p is the pole-arc coefficient.

Considering (18) as fundamental (h = 1), thus P_h can be given in the following form:

$$P_h = \left(\frac{B_{sym}}{B_m}\right)^2 k_{ph}P_{h1} \quad (22)$$

$$k_{ph} = \sum_{h=3,5,7}^{\infty}\frac{k_{tf}(h)^2 k_{sw}(h)V_t + k_{yf}(h)^2 k_{sw}(h)^2 V_y}{k_{tf}(1)^2 k_{sw}(1)V_t + k_{yf}(1)^2 k_{sw}(1)^2 V_y} \quad (23)$$

Preprints (www.preprints.org) | NOT PEER-REVIEWED | Posted: 24 October 2017 doi:10.20944/preprints201710.0155.v1

Peer-reviewed version available at Machines 2017, 5, 30; doi:10.3390/machines5040030

k_{ph} as a harmonic constant is employed to include the harmonic magnetic induction range which can be known from the machine design parameters. Afterwards, a harmonic voltage U_{ph} is used which is

$$U_{ph} = \omega(\lambda_m - L_{ad} I_{ad}) \frac{B_{sym}}{B_m} \tag{24}$$

Regarding to the armature reaction air-gap magnetic induction, the equivalent factors are affiliated with the machines' parameters like equations (25-26) which are coupled with the *d-q* axis equivalent circuit as:

$$\begin{cases} B_{ad1} = \dfrac{\mu_0}{g}\left(1 - \dfrac{4}{\pi} k_U k_{pe}(1)\right) F_{s1} \cos(\psi_1) \propto L_{ad} I_d \\ B_{m1} = \dfrac{4}{\pi} k_{sw}(1) B_m \propto \lambda_m \end{cases} \tag{25}$$

To simplifying the harmonic voltage equation (24), the combination of equations (24 and 25) is resulted into the new fundamental (h=1) expression as given:

$$U_{ph} = \omega\left(\lambda_m - \frac{4}{\pi} k_{sw}(1)\right) \frac{k_U . k_{pe}(1)}{1 - \dfrac{4}{\pi} k_U . k_{pe}(1)} L_{ad}(I_d - \omega I_{ad}) \tag{26}$$

By adopting the harmonic voltage U_{ph}, the harmonic loss P_h (22) can be simplified into the formula of U_{ph} and k_{ph} as follows:

$$P_h = \frac{3}{2}\left(\frac{k_{ph} U_{ph}^2}{R_{ce}}\right) \tag{27}$$

The total stator core resistance (R_c) comprised of eddy-current loss resistance (R_{ce}) and hysteresis loss resistance (R_{ch}), where R_{ce} is eddy-current loss resistance which depends on the type of used material, its dimensions and other machines' design factors. To calculate resistance component of eddy-current and hysteresis losses, the following data are needed to define equations (29 and 30), iron loss based on geometry (such as the yoke and teeth volumes, and material density) and the magnetic induction of each part. Additionally, the expressions of R_{ce} and R_{ch} are validated in reference [27].

$$\frac{1}{R_c} = \frac{1}{n.R_{ch}} + \frac{1}{R_{ce}} \tag{28}$$

$$R_{ch} = \frac{20 a_1 (V_t k_{tf}(1)^2 + V_y k_{yf}(1)^2) B_{m1}^2}{\rho(\pi\lambda_m)^2} \tag{29}$$

$$R_{ce} = \frac{a_2 B_{m1}^2 k_{tf}(1)^2 V_t (1 + a_3 B_{m1}^{a_4}) + a_2 B_{m1}^2 k_{yf}(1)^2 V_y (1 + a_3 B_{m1}^{a_4})}{6(\pi\lambda_m)^2} \tag{30}$$

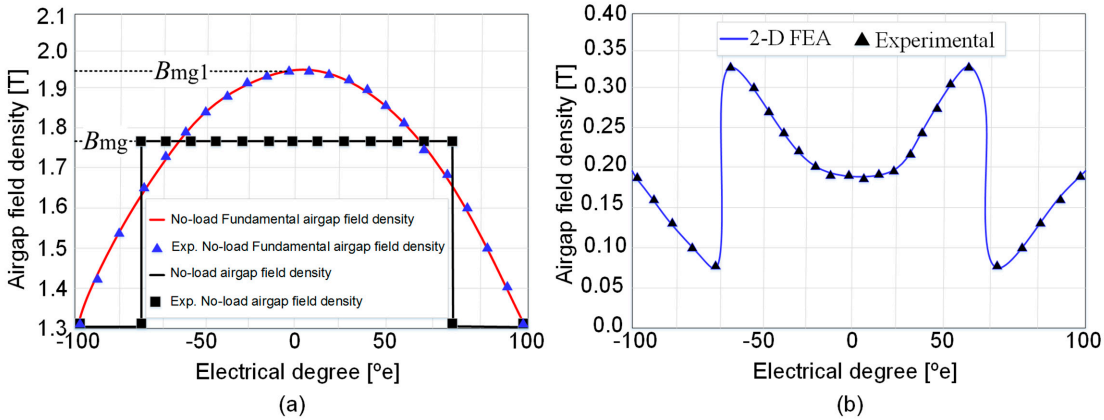

Figure 3 Comparison of no-load air-gap magnetic field density: (**a**) field density waveform; (**b**) field density harmonic waveforms.

Preprints (www.preprints.org) | NOT PEER-REVIEWED | Posted: 24 October 2017 doi:10.20944/preprints201710.0155.v1

Peer-reviewed version available at Machines 2017, 5, 30; doi:10.3390/machines5040030

3. RESULTS AND DISCUSSION

After the analytical and numerical modelling by the modified IEM-Formula, a wide region of FWOT is observed. Hence, a significant harmonic loss is produced which causes a considerable increase in iron loss. Since a large deviation in iron loss prediction using the classic IEM-Formula can be seen in comparison with test's results, an IEM-Formula-based modification on the equivalent circuit of the PMSM is proposed to consider harmonic losses.

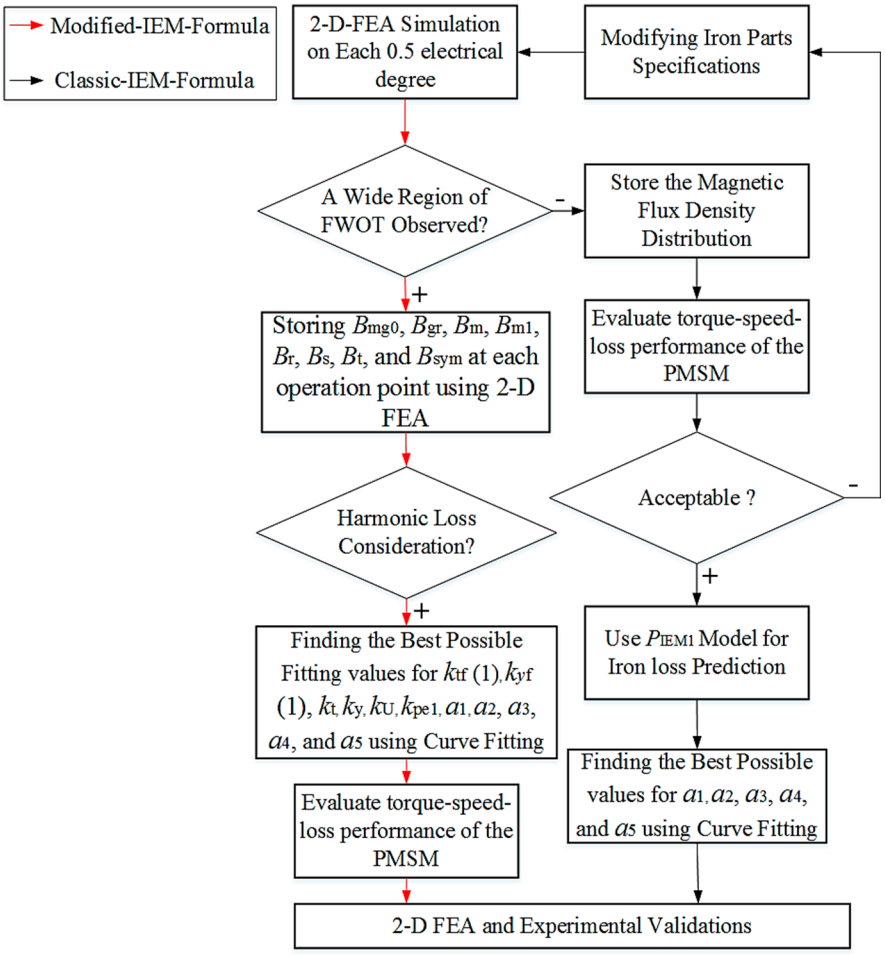

Figure 4 Flowchart of the analysis dynamic.

Table 1. Specifications of the proposed PMSM

Parameters	Values	Units
Stator outer/ inner diameters	209/115	mm
Rotor outer/ inner diameters	230/217	mm
Axial length	100	mm
Slots/ poles =SP	36/40=0.9	
Air-gap length	1.0	mm
Magnet thickness	8.0	mm
Magnet pole-arc	100	^{o}e
Rated power	6.0	kW
Rated speed	200	rpm
DC link voltage	320	V

Preprints (www.preprints.org) | NOT PEER-REVIEWED | Posted: 24 October 2017 doi:10.20944/preprints201710.0155.v1

Peer-reviewed version available at Machines 2017, 5, 30; doi:10.3390/machines5040030

Steel sheet's type	M400-50A	
Lamination length	95	mm

Figure 4 contains a flowchart illustrating the calculations on a fractional-slot concentrated winding, radial field permanent magnet machine with 6 kW rated power in generator-mode. The figure also shows the results of the analysis during FWOT. The total iron loss using classic IEM-Formula (red curve) sharply diverges; however, the modified IEM-Formula (green curve) along with the experimental results rapidly increase during FWOT.

Table I presents the sizeable dimensions and specifications of the prototype PMSM. Table II illustrates the value of the coefficients.

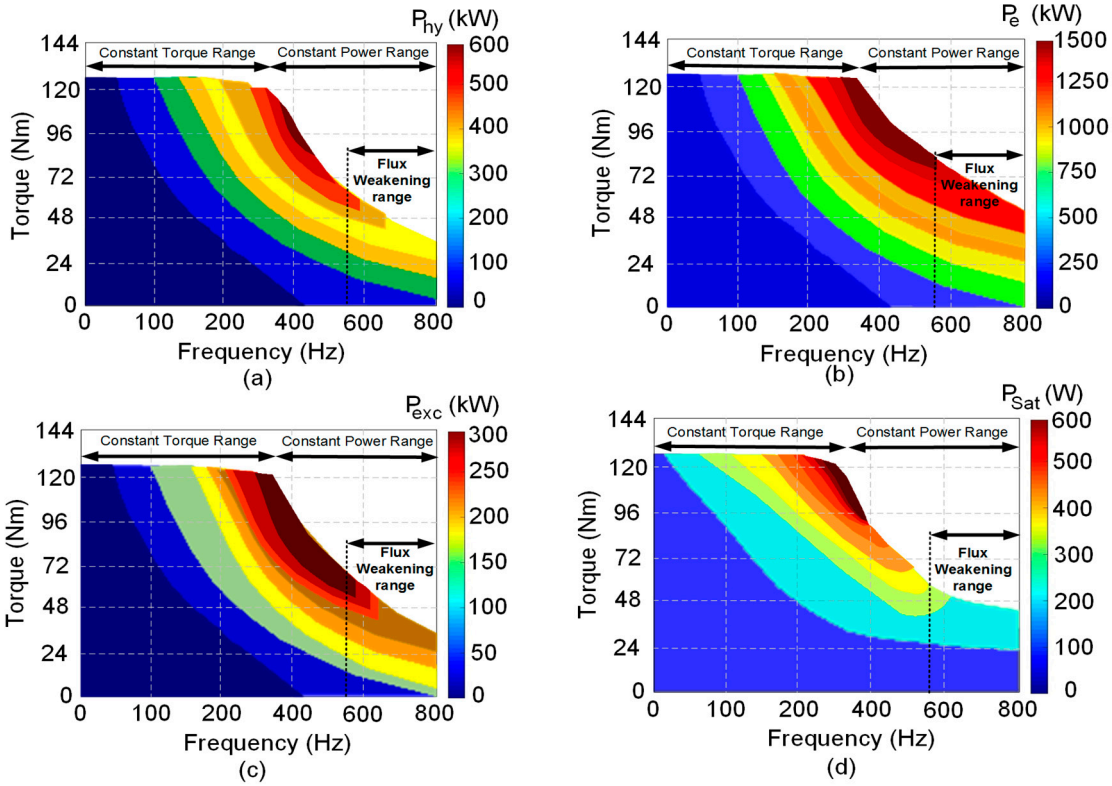

Figure 5 Predicted iron losses using modified IEM-Formula as function of torque and frequency, where: (**a**) the Hysteresis loss; (**b**) the eddy-current loss; (**c**) Excess loss contribution; and (**d**) saturation loss.

First, a large range of FWOT is observed and the previously mentioned magnetic field density components are stored using 2-D FEA for each 0.5 electrical degree. Second, the coefficients are calculated using a curve fitting technique based on the multi-generalized reduced gradient nonlinear (M-RGN) method [33].

Figure 5 illustrates the behavior of torque-frequency-loss of the machine, in which the terms of the iron loss such as hysteresis, eddy-current, excess, saturation, and harmonic are calculated from the modified IEM-Formula. The Hysteresis loss (Figure 5-a), eddy-current loss (Figure 5-b), excess loss (Figure 5-c), and saturation loss (Figure 5-d) are shown based on their constant torque and power range with a considerable field weakening region.

Figure 6-a proves the generated harmonics perspective of eddy-current and total iron losses by the classic and modified-IEM-Formula. A considerable difference in the total iron loss and also efficiency during FWOT can be seen between the two methods. Figure 6-b shows how the following terms in Figure 6-a are representing the total iron loss prediction based on torque-frequency-loss evaluation.

Preprints (www.preprints.org) | NOT PEER-REVIEWED | Posted: 24 October 2017 doi:10.20944/preprints201710.0155.v1

Peer-reviewed version available at Machines 2017, 5, 30; doi:10.3390/machines5040030

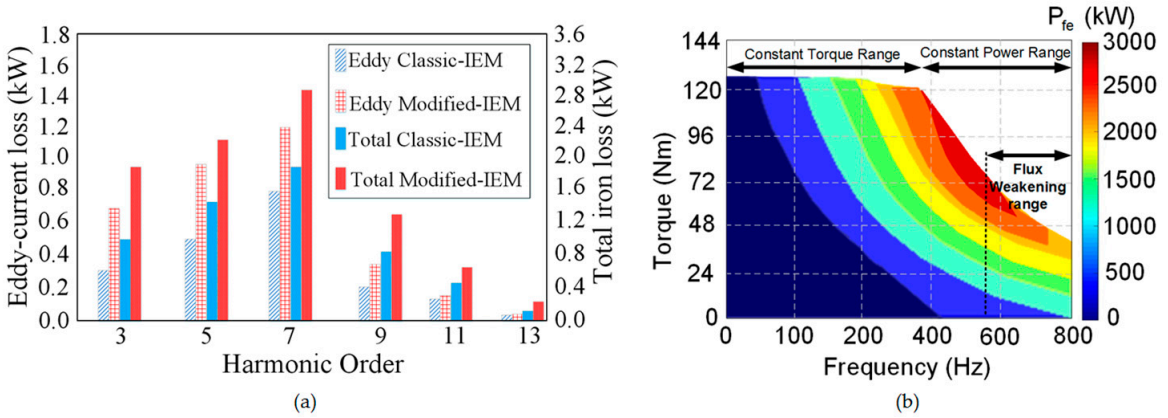

Figure 6 Harmonic spectra and total iron loss prediction using classic and modified IEM-Formula during FWOT, where: (**a**) existing dominant harmonics on total iron loss and specially eddy current loss; (**b**) presentation of the torque-frequency-power loss by the modified IEM-Formula

Table 2. Coefficients calculation using the modified IEM-Formula by curve fitting

Coefficients	Values	Units
k_{tf} (1)	7.0439E-01	
k_{yf} (1)	7.7938E-01	
k_t	0.4567	
k_y	0.3031	
k_{pe} (1)	0.3991	
k_U	0.4586	
a_1	398.0363203	W/m^3
a_2	2.3821E-02	W/m^3
α	1.705944	
a_3	11.74239805	W/m^3
a_4	8.27E-02	
a_5	1.3617E-09	W/m^3

4. EXPERIMENTAL VERIFICATION

A surface mounted permanent magnet synchronous generator with 36 slots for a vast operating range of 6 kW (nominal power) is manufactured with the listed sizeable dimensions and specifications which reported in Table I. The stator and rotor cores both are made of M400-50A steel sheet. The modified IEM-Formulas' coefficients are extracted by numerical fitting the no-load experiment results combined with FEA results. The no-load iron loss is measured through the difference between the total no-load loss and mechanical loss. First, the prototype SPMSM is dragged under no-load condition, and tested the total no-load loss curve verse the speed. This total no-load loss P_{fe} (total) consists of the no-load iron loss P_{fe} and the mechanical loss P_{mech}. The SPMSG under test is fed by a variable-speed frequency converter (ABB ACS600) and loaded by a DC machine (prime mover). The shaft torque is measured by a torque transducer (TORQUEMASTER TM-214). The electrical power (input/ and output) are measured by a power analyzer (Yokogawa PZ4000). Afterwards, all the data (such as voltage, torque, power, and efficiency) were stored by a reading unit to the laboratories' computer. The prototype machine is designed particularly for laboratory test use. As the output power is stored by a dynamometer. Thus, the total loss (consists of copper, iron, and mechanical losses) has been obtained by a simple subtract between input and output powers. The copper loss has been

Preprints (www.preprints.org) | NOT PEER-REVIEWED | Posted: 24 October 2017 doi:10.20944/preprints201710.0155.v1

Peer-reviewed version available at Machines 2017, 5, 30; doi:10.3390/machines5040030

calculated via the measured phase current and resistance, as well as the mechanical loss was provided in the coefficient extracting experiment.

Figure 7-a demonstrates the stator and rotor cores, and the two PI-PWM units as a part of the control system in a wind power application, in which a vertical-axis wind turbine is employed [34]. A test bench prototyping platform composed of a 6 kW synchronous wind generator with a 1024 points absolute encoder, current sensors and a power brake controlled load is also shown in Figure 7-b.

Figure 8 illustrates the influence of the modified IEM-Formula on the total iron loss and efficiency with 3-D FEA and experimental verifications for the studied PMSG. From the standpoint of the classic IEM-Formula model, the iron loss resistance is the parallel connection of the hysteresis losses and the eddy-current losses. This is examined through the air-gap field density with the motor speed as the operation parameter. While the SPMSM operates in the field weakening region, the terminal voltage remains changeless because it is diminished by the DC link voltage. As predicted by the classic IEM-Formula model, the iron loss resistance rises with the speed, shown in (18). Thus, the iron loss decreases in a similar manner during field weakening operation. However, this predicted result is far from the results from the experiments and FEA calculation. This is due to the fact that large eddy-current loss is generated during field weakening, rapidly decreasing the efficiency of the machine. Figure 8-a shows the comparison of iron loss obtained by the proposed PMSM for the classic IEM-Formula, the proposed modified

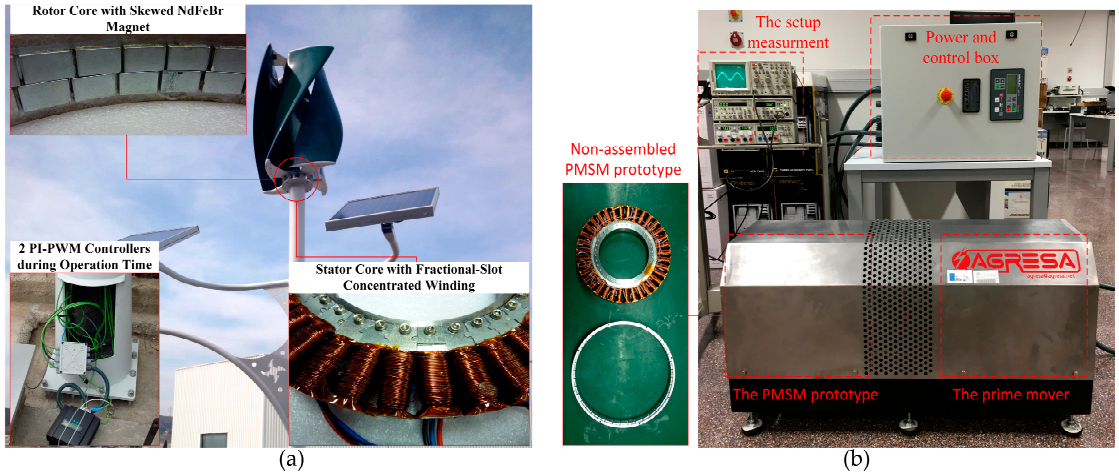

Figure 7 Experimental investigation, where: (**a**) the proposed PMSM with non-assembled parts under operation; (**b**) experimental setup

IEM-Formula, 3-D FEA and experimental measurement. The classic IEM-Formula shows significant deviation during FWOT from the modified formula. The classic IEM-Formula shows significant deviation during FWOT from the modified formula which shows worthy agreement with experimental and 3-D FEA results. This result presents that the harmonic loss must be considered if a wide FWOT exists. Figure 8-b presents how the efficiency calculation might create a considerable error during FWOT. The error between the proposed model and experiment results is due to neglecting the slot opening effect and fringing effect. Whereas, the iron loss predicted by the classic IEM-Formula is obviously underestimated, particularly during the field weakening region due to ignoring the harmonic loss.

Preprints (www.preprints.org) | NOT PEER-REVIEWED | Posted: 24 October 2017 doi:10.20944/preprints201710.0155.v1

Peer-reviewed version available at Machines 2017, 5, 30; doi:10.3390/machines5040030

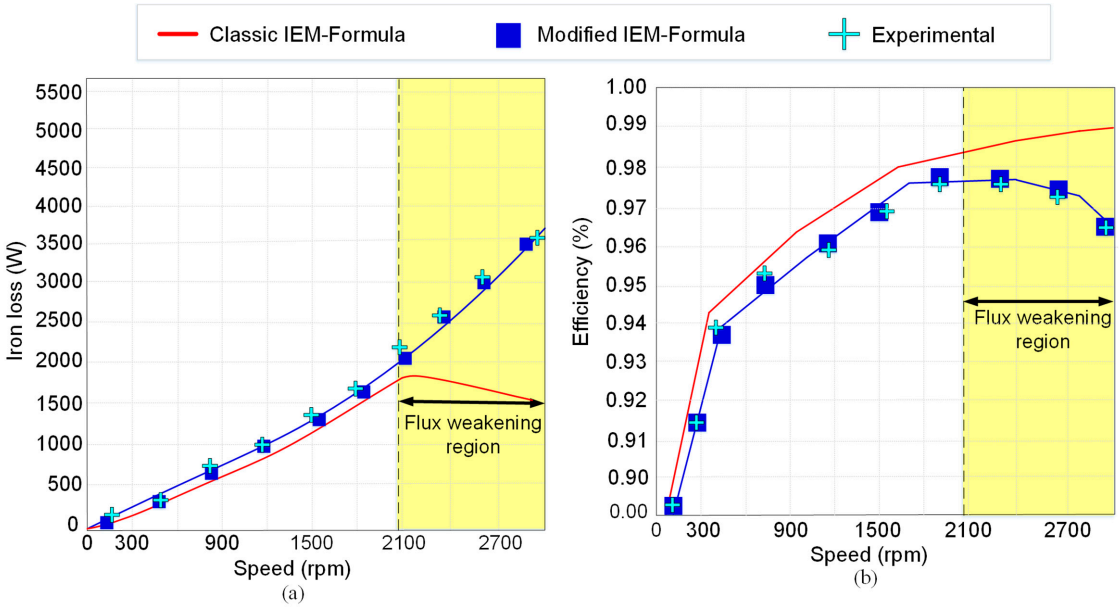

Figure 8 Comparison of classic IEM-Formula with modified IEM-Formula during FWOT, where: (**a**) shows total iron loss evaluation; (**b**) presents efficiency computation.

4. Conclusions

The main contribution of this work is to propose an analytical modelling procedure of iron loss prediction which uses classic IEM-Formula for an accurate iron loss and efficiency prediction during the field weakening operation. We modelled harmonic loss based on an equivalent circuit without any circuit assumption in addition to the other terms and the outcome interpreted how significantly the behavior of the PMSM was influenced during this wide FWOT. Regarding to the findings, a large error can remain in the analysis process, if classic IEM-Formula is used, due to phase current harmonic. In other words, the core resistance rises dramatically and a considerable voltage drop causes larger harmonic loss and consequently the total iron loss under FWOT condition. The proposed modified IEM-Formula is also experimentally tested on a permanent magnet synchronous generator with a double-layer fractional-slot concentrated winding for a small power wind energy harvesting in the coast of Barcelona city. A qualified agreement is achieved between proposed analytical iron loss, numerical models and experimental results. Additionally, this research has ignored the effects of slot opening and fringing with minimal effect on the predicted losses. Moreover, commercial and environmental issues of the project have been highly considered to reduce CO_2 emissions as a part of green power generation projects.

References

1. S. Steentjes; et al.. Iron-Loss Model With Consideration of Minor Loops Applied to FE-Simulations of Electrical Machines. *IEEE Trans. Magn.*, vol. 49, no. 7, pp. 3945–3948, July. 2013.
2. D. Eggers; et al., .Advanced Iron-Loss Estimation for Nonlinear Material Behavior. *IEEE Trans. Magn.*, vol. 48, no. 11, pp. 3021–3024, Nov. 2012.
3. N. Alatawneh; et al.. Accuracy of time domain extension formulae of core losses in non-oriented electrical steel laminations under non-sinusoidal excitation. *IET Electric Power App.*, doi: 10.1049/iet-epa.2016.0737, vol. 11, no. 6, pp. 1131– 1139, Nov. 2017.
4. A. Krings; and J. Soulard. Overview and comparison of iron loss models for electrical machines. *Journal of Electrical Engineering*, vol. 10, no. 3, pp. 162–169, 2010.
5. D. M. Ionel; M. Popescu; S. J. Dellinger; T. J. E. Miller; R. J. Heideman; and M. I. McGilp. On the variation with flux and frequency of the core loss coefficients in electrical machines. *IEEE Trans. Ind. Appl.*, vol. 42, no. 3, pp. 658–667, May 2006.

6. D. M. Ionel; M. Popescu; M. I. McGilp; T. J. E. Miller; S. J. Dellinger; and R. J. Heideman. Computation of Core Losses in Electrical Machines Using Improved Models for Laminated Steel," *IEEE Trans. Ind. Appl.*, vol. 43, no. 6, pp. 1554–1564, Nov. 2007.
7. A. D. Gerlando; and R. Perini. Evaluation of the Effects of the Voltage Harmonics on the Extra Iron Losses in the Inverter Fed Electromagnetic Devices. *IEEE Trans. on Energy Conversion*, Vol. 14, No. 1, pp. 57-62, March 1999.
8. J. Kim; I. Jeong; K. Nam; J. Yang; and T. Hwang. Sensorless control of PMSM in a high-speed region considering iron loss. *IEEE Trans. Ind. Electron.*, vol. 62, no. 10, pp. 6151–6159, Oct. 2015.
9. P. Rasilo; et al.. Experimental determination and numerical evaluation of core losses in a 150-kVA wound-field synchronous machine. *IET Electric Power App.*, doi: 10.1049/iet-epa.2012.0242, vol. 7, no. 2, pp. 97–105, 2013.
10. Z. Haisen; et al.. Piecewise variable parameter model for precise analysis of iron losses in induction motors. *IET Electric Power App.*, doi: 10.1049/iet-epa.2016.0009, vol. 11, no. 3, pp. 361–368, 2017.
11. S.-H. Han; W. L. Soong; T. M. Jahns; M. K. Guven; and M. S. Illindala. Reducing harmonic eddy-current loss in the stator teeth of interior permanent magnet synchronous machines during flux weakening. *IEEE Trans. Energy Conversion*, vol. 25, no. 2, pp. 441–449, Jun. 2010.
12. L. Qi; et al.. Stator teeth eddy-current loss analysis of interior permanent magnet machine during flux weakening. *IEEE International Conference on Electrical Machines and Systems (ICEMS)*, DOI: 10.1109/ICEMS.2013.6713370, pp. 1226–1230, 2013.
13. Y. Yokoi; et al.. General formulation of winding factor for fractional-slot concentrated winding design. *IET Electric Power App.*, doi: 10.1049/iet-epa.2014.0336, vol. 10, no. 4, pp. 231–239, 2015.
14. L. Yue; et al.. Increasing the saliency ratio of fractional slot concentrated winding interior permanent magnet synchronous motors. *IET Electric Power App.*, doi: 10.1049/iet-epa.2015.0092, vol. 9, no. 7, pp. 439–448, 2015.
15. J. Kim; I. Jeong; K. Nam; J. Yang; and T. Hwang. Sensorless control of PMSM in a high-speed region considering iron loss. *IEEE Trans. Ind. Electron.*, vol. 62, no. 10, pp. 6151–6159, Oct. 2015.
16. K. Yamazaki. Torque and efficiency calculation of an interior permanent magnet motor considering harmonic iron losses of both the stator and rotor. *IEEE Trans. Magn.*, vol. 39, no. 3, pp. 1460–1463, May 2003.
17. K. Akatsu; K. Narita; Y. Sakashita; and T. Yamada. .Impact of flux weakening current to the iron loss in an IPMSM including PWM carrier effect. *in Proc. IEEE Energy Conversion. Congr. Expo.*, San Jose, CA, USA, Sep. 2009, pp. 1927–1932.
18. K. Yamazaki; and H. Ishigami. Rotor-shape optimization of interior permanent-magnet motors to reduce harmonic iron losses. *IEEE Trans. Ind. Electron.*, vol. 57, no. 1, pp. 61–69, Jan. 2010.
19. K. Yamazaki; M. Kumagai; T. Ikemi; and S. Ohki. A novel rotor design of interior permanent-magnet synchronous motors to cope with both maximum torque and iron-loss reduction. *IEEE Trans. Ind. Appl.*, vol. 49, no. 6, pp. 2478–2486, Nov/Dec. 2013.
20. S. Kuttler; et al.. Fast iron losses model of stator taking into account the flux weakening mode for the optimal sizing of high speed permanent internal magnet synchronous machine. *Elsevier Journal, Mathematics and Computers in Simulation*, 131 (2017) 328-343, pp. 1–15, 2017.
21. A. Tessarolo; et al.. Modeling, Analysis, and Testing of a Novel Spoke-Type Interior Permanent Magnet Motor With Improved Flux Weakening Capability. *IEEE Trans. on Magnetics*, VOL. 51, NO. 4, MAY 2017, pp.1-9, 2015.
22. S. Atiq; and B. Kwon. Susceptibility of the winding switching technique for flux weakening to harmonics and the choice of a suitable drive topology. *International journal of electrical power and energy systems (Elsevier Journal)*, https://doi.org/10.1016/j.ijepes.2016.07.001, VOL. 85, pp.22-31, 2017.
23. M. Rekik; et al.. Improvement in the field-weakening performance of switched reluctance machine with continuous mode. *IET Electric Power App.*, doi: 10.1049/iet-epa.2015.0092, vol. 9, no. 7, pp. 439–448, 2015.
24. S. Vaez-Zadeh; and B. Zahedi. Modeling and analysis of variable speed single phase induction motors with iron loss. *Energy Conversion and Management (Elsevier Journal)*, doi:10.1016/j.enconman.2009.06.031, VOL. 50, No. 11, pp. 2747-2753, 2009.
25. M. Basic; et al.. Dynamic and pole-zero analysis of self-excited induction generator using a novel model with iron losses. *International journal of electrical power and energy systems (Elsevier Journal)*, https://doi.org/10.1016/j.ijepes.2012.03.003, VOL. 42, pp.105-118, 2015.

26. Q. Li; T. Fan; and X. Wen. Armature-reaction magnetic field analysis for interior permanent magnet motor based on winding function theory. *IEEE Trans. Magn*., vol. 49, no. 3, pp. 1193–1201, Mar. 2013.
27. Q. Li; et al.. Characterization of Iron Loss for Integral-Slot Interior Permanent Magnet Synchronous Machine During Flux Weakening. *IEEE Trans. on Magnetics*, VOL. 53, NO. 5, MAY 2017, pp.1-7, 2017.
28. H. Saavedra; et al.. Detection of inter turn faults in PMSMs with different winding configurations. *Energy Conversion and Management (Elsevier Journal)*, http://dx.doi.org/10.1016/j.enconman.2013.12.059, VOL. 79, pp. 534-542, 2014.
29. P. Donolo; et al.. Analysis of voltage unbalance effects on induction motors with open and closed slots. *Energy Conversion and Management (Elsevier Journal)*, doi:10.1016/j.enconman.2010.10.045, VOL. 52, No. 5, pp. 2024-2030, 2011.
30. Y. Ueda; et al.. Instrument for real-time measurements of airgap flux distribution of on-load synchronous generators. *IEE Proceedings A-Physical (IET)*, DOI: 10.1049/ip-a-1:19870047, Vol. 134, Issue: 4, pp. 331-334, 1987.
31. J. R. Hendershot; and T. J. E. Miller. Design and Performance of Brushless Permanent-Magnet Motors. London, U.K.: Oxford Univ. Press, 1994.
32. V. Životi´; c-Kukolj; W. L. Soong; and N. Ertugrul. Iron loss reduction in an interior PM automotive alternator *IEEE Trans. Ind*. Appl., vol. 42, No. 6, pp. 1478–1486, Nov./Dec. 2006.
33. L. S. Lasdon; et al.. Design and testing of a generalized reduced gradient code for nonlinear optimization. Case Western Reserve University, National Technical Information Service U. S. Department of Commerce (NTIS), AD-A009-402, pp.1-45, March 1975.
34. S. M. Muyeen, et al., "Variable speed wind turbine generator system with current controlled voltage source inverter. *Energy Conversion and Management (Elsevier Journal)*, doi:10.1016/j.enconman.2011.02.001, VOL. 52, pp. 2688-2694, 2011.